SAND2019-5739C

Generalized Entropy Stable Weighted Essentially Non-Oscillatory Finite Difference Scheme in Multi-Block Domains

J. Brad Maeng * and Travis C. Fisher†
Sandia National Laboratories, Albuquerque, NM 87123

Mark H. Carpenter‡
NASA Langley Research Center, Hampton, VA 23681

A new cell-centered third-order entropy stable Weighted Essentially Non-Oscillatory (SSWENO) finite difference scheme in multi-block domains is developed for compressible flows. This new scheme overcomes shortcomings of the conventional SSWENO finite difference scheme in multi-domain problems by incorporating non-dissipative Simultaneous Approximation Term (SAT) penalties into the construction of a dual flux. The stencil of the generalized dual flux allows for full stencil biasing across the interface while maintaining the nonlinear stability estimate. We demonstrate the shock capturing improvement across multi-block domain interfaces using the generalized SSWENO in comparison to the conventional entropy stable high-order finite difference with interface penalty in shock problems. Furthermore, we test the new scheme in multi-dimensional turbulent flow problems to assess the accuracy and stability of the multi-block domain formulation.

I. Introduction

High-fidelity simulations have been taking a more decisive role in the design and analysis of complex engineering systems in recent times. These types of simulations allow engineers to push the envelope of extreme flow physics where no experimental means are available or just too expensive to conduct experiments. Especially, in computational fluid dynamics simulations of compressible turbulent flows, they have become an indispensable tool to study unsteady flows in and around complex geometries, and in extreme environments. Even though recent advances in computer architectures and computing power have made larger simulations possible, these advances alone are not sufficient to fully demonstrate high-fidelity simulations of large-scale compressible flows without proper numerical tools.

Many state-of-the-art high-fidelity simulations, such as Direct Numerical Simulation (DNS) or Large Eddy Simulation (LES), utilize high-order numerical methods to efficiently compute and capture details in turbulent flows. Unlike low-order schemes, high-order numerical methods often lose robustness in the presence of strong nonlinear flow features. These nonlinearities could alter the behavior of the solution, or worse, terminate a simulation prematurely. Various nonlinear stabilization methods have been developed in order to address this issue. Such techniques include flux limiting, filtering, solution reconstruction-based methods like Weighted Essentially Non-Oscillatory and more. Although these methods can mitigate adverse effect of strong gradients and spurious oscillations in flow solutions, constructing these in a mathematically rigorous and provable manner has been difficult to achieve.

The summation-by-parts (SBP) framework with the simultaneous approximation term (SAT) penalties [1] allows us to design high-order difference operators that are conservative in finite domains and ensures consistency of the resulting numerical method. With entropy stability analysis, we can design high-order methods that are conservative, consistent and, importantly, provably stable. The resulting high-order numerical operators can provide an indispensable tool to achieve stable high-fidelity computational fluid dynamics simulations. A provably entropy stable high-order finite difference scheme was first introduced by Fisher and Carpenter [2] for the Navier-Stokes equations in finite domains. They used the entropy stable dual-flux form satisfying the SBP property to construct the entropy stable Weighted Essentially Non-Oscillatory scheme and demonstrated provable stability in the presence of strong discontinuities and in turbulent flow applications.

---

[*] Senior Member of Technical Staff, Computational Thermal and Fluid Mechanics, MS 0828, AIAA Member

[†] Principal Member of Technical Staff, Computational Thermal and Fluid Mechanics, MS 0828, AIAA Senior Member

[‡] Senior Research Scientist, Computational Aerosciences

While it is possible to extend the entropy stable SAT penalty approach in [2] with the entropy stable WENO scheme across discontinuous interfaces, the resulting multi-block domain coupling from the conventional SBP only does so weakly due to the collocated nature of solution and flux points on boundaries. Yamaleev and Carpenter [3] have applied an approach to address this for the conventional operator in spectral collocation schemes by incorporating upwinded SAT penalties into the divergence operator and forming a WENO operator that exhibits some ability to apply stencil biasing across domains. In this work we use the naturally stronger coupling that results from moving the solution points into the domain interior and use non-dissipative SAT penalties to form a fully-coupled WENO operator with extensive stencil biasing across the interface. The new generalized SBP framework allows solution and flux points to be specified uniquely on the boundaries, similar to the cell-centered finite volume scheme, and will be shown to perform robustly. We believe that the generalized entropy stable finite differences will be considerably beneficial for high-speed flow simulations in curvilinear multi-block domains.

In the following sections, we present a new cell-centered third-order entropy consistent SBP operator and entropy stable WENO finite difference scheme applied to multi-block compressible flow applications. We begin by reviewing the entropy stable high-order finite difference method and entropy stability. Then, we introduce the generalized entropy stable interface coupling. We present verification and demonstrations of the scheme in one- and multi-dimensional test problems to test and assess the scheme's ability to capture strong shocks and resolve turbulent flows.

II. Governing Equations

In this study, we consider the calorically perfect compressible Euler equations in three dimensions in the form

$$\begin{aligned} \mathbf{u}_t + (\mathbf{f}_k)_{x_k} &= 0,\ \ x_k \in \Omega,\ \ t \in [0,\infty), \\ \mathbb{B}(\mathbf{u}) &= \mathbf{g}^{bnd},\ \ x_k \in \partial\Omega,\ \ t \in [0,\infty), \\ \mathbf{u}(x,0) &= \mathbf{g}_0(x_k),\ \ x_k \in \Omega, \end{aligned} \tag{1}$$

where $\mathbf{u} = (\rho, \rho v_i, \rho E)^T$ is a conserved variable vector, $x_k = (x, y, z)$ is the cartesian coordinates, $\mathbf{f}_k$ is the conserved inviscid flux vector, and $v_i = (u, v, w)^T$ is the velocity vector. The boundary vector $\mathbf{g}^{bnd}$ is assumed to be well-posed data. The inviscid flux vector is

$$\mathbf{f}_k = \left(\rho v_i, \rho v_1 v_k + p\delta_{1k}, \rho v_2 v_k + p\delta_{2k}, \rho v_3 v_k + p\delta_{3k}, \rho v_k H\right)^T, \tag{2}$$

where $H = E + \frac{p}{\rho}$ is the total enthalpy. The equation of state for the system is $p = \rho e(\gamma - 1)$.

III. Entropy Stable High-Order Finite Difference

We describe the methodologies to construct the entropy stable high-order finite difference scheme.

A. Complementary Grid and Telescopic Flux Form

Complementary grids allow the finite differences to be expressed as simple flux differences. This property is commonly referred to as the telescopic flux property and is important in satisfying the convergence of numerical solution to a weak solution. We define the computational domain where N equally spaced solution points are defined

$$\mathbf{x} = (x_1, x_2, \ldots, x_N)^T, \quad x_i = x_L + \left(\frac{1}{2N} + \frac{i-1}{N}\right)(x_R - x_L), \quad i = 1, \ldots, N. \tag{3}$$

The flux points are defined at the boundaries of control volumes with the solution points not necessarily at the centroid. There are $N + 1$ flux points for N solution points. In high-order finite difference methods, these flux points are equally distributed in the domain interior, however, the spacing becomes irregular near the boundaries. The spacing between flux points is defined by the following relation.

$$\bar{\mathbf{x}} = (\bar{x}_0, \ldots, \bar{x}_N)^T, \quad \Delta\bar{\mathbf{x}} = \mathcal{P}\mathbf{I}, \tag{4}$$

where the differencing operator Δ is an $N \times (N+1)$ matrix

$$\Delta = \begin{pmatrix} -1 & 1 & 0 & 0 & 0 & 0 \\ 0 & -1 & 1 & 0 & 0 & 0 \\ \vdots & \ddots & \ddots & \ddots & \ddots & \vdots \\ 0 & 0 & 0 & -1 & 1 & 0 \\ 0 & 0 & 0 & 0 & -1 & 1 \end{pmatrix}, \tag{5}$$

and $\mathcal{P}$ is a diagonal matrix whose entries contain the spacing norm between flux points.

The complementary grid enables us to express the spatial derivatives in telescopic flux form, with some manipulation, as

$$f(u)_x = \mathcal{P}^{-1}\Delta\bar{\mathbf{f}} = \mathcal{P}^{-1}\mathcal{Q}\mathbf{f}. \tag{6}$$

where $\mathcal{Q}$ is a first derivative operator that satisfies the summation-by-parts (SBP) property and is described in the following section. Operators that satisfy the generalized SBP property lead to consistent end fluxes, thus admit the telescopic flux property.

B. Summation-By-Parts Operators

Summation-by-parts (SBP) operators [1] are used to approximate derivatives in high-order finite difference schemes. We lay out the first derivative operator used in this work. The first derivative approximation, $\mathcal{D}\phi$, is constructed as follows.

$$\begin{aligned} &\mathcal{D} = \mathcal{P}^{-1}\mathcal{Q}, \quad \mathcal{P} = \mathcal{P}^T, \quad \boldsymbol{\xi}^T\mathcal{P}\boldsymbol{\xi} > 0, \quad \boldsymbol{\xi} \neq 0 \\ &\mathcal{Q}^T = \mathcal{B} - \mathcal{Q}. \end{aligned} \tag{7}$$

The spacing norm matrix $\mathcal{P}$, which is restricted to the diagonal form for our application, contains the local grid spacing information. The nearly skew-symmetric matrix $\mathcal{Q}$ is an undivided differencing operator where all rows sum to zero.

We define $\mathcal{B}$ for generalized SBP as

$$\mathcal{B} = \mathbf{b}_1\mathbf{b}_1^T - \mathbf{b}_{-1}\mathbf{b}_{-1}^T, \tag{8}$$

which depends on the boundary interpolation vector $\mathbf{b}$. The subscripts, -1 and 1, denote the left and right boundary in the domain. Thus, the i^{th} component of $\mathbf{b}_{-1}$ is equivalent to the $(N+1-i)^{th}$ component of $\mathbf{b}_1$

$$\mathbf{b}_{-1,(i)} = \mathbf{b}_{1,(N+1-i)}, \quad i = 0, \dots, N. \tag{9}$$

The boundary interpolation vector $\mathbf{b}$ determines how end flux points are defined. For the conventional nodal finite difference scheme, the SBP boundary vector is defined as

$$\mathbf{b}_{-1} = (1, 0, \dots, 0)^T, \quad \mathbf{b}_1 = (0, \dots, 0, 1)^T \tag{10}$$

where the outer-most boundary SBP points coincide with the finite domain solution points at boundaries. Thus, $\mathcal{B}$ only contains the first and the last entries of the diagonal matrix $\mathcal{B} = \mathrm{diag}(-1, 0, \dots, 0, 1)$. However, for generalized SBP, the outer-most boundary SBP points may not coincide with the outer-most solution points. This is achieved by the use of boundary interpolation vector.

$$\mathbf{b}_{-1} = (b_1, b_2, \dots, b_{n_b}, \dots 0)^T, \quad \mathbf{b}_1 = (0, \dots, b_{n_b}, \dots, b_2, b_1)^T, \tag{11}$$

where n_b refers to the number of points used in the interpolation of boundary points.

The first derivative approximation satisfying the SBP property mimics the integration-by-parts

$$\int_{x_L}^{x_R} \phi u_x dx = \phi u_x|_{x_L}^{x_R} - \int_{x_L}^{x_R} \phi_x u dx, \tag{12}$$

discretely as

$$\boldsymbol{\phi}^T\mathcal{P}\mathcal{D}\mathbf{u} = \boldsymbol{\phi}^T\mathcal{P}\mathcal{P}^{-1}(\mathcal{B} - \mathcal{Q}^T)\mathbf{u} = \boldsymbol{\phi}\mathbf{b}_1\mathbf{b}_1^T\mathbf{u} - \boldsymbol{\phi}\mathbf{b}_{-1}\mathbf{b}_{-1}^T\mathbf{u} - \boldsymbol{\phi}^T\mathcal{D}^T\mathcal{P}\mathbf{u}, \tag{13}$$

where $\boldsymbol{\phi} = (\phi_1, \ldots, \phi_N)^T$.

The (2-4-2) SBP operator[*] is presented for the generalized cell-centered high-order finite difference scheme. For the boundary interpolant defined by

$$\mathbf{b}_{-1} = \left(\frac{35}{16}, -\frac{35}{16}, \frac{21}{16}, -\frac{5}{16}, 0, \ldots, 0\right)^T, \tag{14}$$

we have the following unique spacing norm and the differencing operators

$$\mathcal{P} = \operatorname{diag}\left(\frac{433}{384}, \frac{95}{128}, \frac{451}{384}, \frac{367}{384}, 1, \ldots, 1, \frac{367}{384}, \frac{451}{384}, \frac{95}{384}, \frac{433}{384}\right)\delta x, \tag{15}$$

$$Q = \begin{pmatrix} -\frac{1225}{512} & \frac{6695}{1536} & -\frac{4097}{1536} & \frac{359}{512} & 0 & 0 & 0 & \ldots \\ \frac{655}{1536} & -\frac{1225}{512} & \frac{1415}{512} & -\frac{1225}{1536} & 0 & 0 & 0 & \ldots \\ -\frac{313}{1536} & \frac{55}{512} & -\frac{441}{512} & \frac{533}{512} & -\frac{1}{12} & 0 & 0 & \ldots \\ -\frac{9}{512} & \frac{175}{1536} & -\frac{323}{512} & -\frac{25}{512} & \frac{2}{3} & -\frac{1}{12} & 0 & \ldots \\ 0 & 0 & \frac{1}{12} & -\frac{2}{3} & 0 & \frac{2}{3} & -\frac{1}{12} & \ldots \\ \vdots & \vdots & \vdots & \ddots & \ddots & \ddots & \ddots & \vdots \end{pmatrix}, \tag{16}$$

where the structure on the left boundary of Q is only shown to demonstrate. The interior coefficients, the last row shown in Eq. (16), are repeated until the right boundary is reached. The same Q structure on the right boundary is assumed.

C. Entropy Stable Finite Difference Scheme

The semi-discrete form of governing equations Eq. (1) in the flux form finite differences is

$$\mathbf{u}_t + \mathcal{P}_k^{-1}\Delta_k \bar{\mathbf{f}}_k = \mathcal{P}_k^{-1}\mathbf{g}_k^{int} + \mathcal{P}^{-1}\mathbf{g}_k^{bnd}, \quad k = 1, 2, 3, \tag{17}$$

where $\mathbf{g}_k^{int}$ and $\mathbf{g}_k^{bnd}$ are the interface and boundary penalty terms. For the following analysis, we drop the subscript k since analysis can be applied in dimension by dimension fashion. The interface penalty is necessary to handle multi-block domain configurations. For the purpose of this work, we disregard any boundary effects and only concern ourselves with the interface effect. However, appropriate boundary penalty treatments can be found elsewhere [4–6].

1. Semi-Discrete Entropy Analysis

The aim of the semi-discrete entropy analysis is to show that the global semi-discrete entropy decay mimics the continuous entropy condition of the conservation law. Details of regarding continuous entropy analysis can be found in [2, 7] and references therein.

The semi-discrete entropy equation of Eq. (17) is

$$\mathbf{w}^T\mathcal{P}\mathbf{u}_t + \mathbf{w}^T\Delta\bar{\mathbf{f}} = \mathbf{w}^T\mathbf{g}^{int} + \mathbf{w}^T\mathbf{g}^{bnd}, \tag{18}$$

where $\mathbf{w} = (w(u_1), \ldots, w(u_N))^T$ is the vector of entropy variables. The diagonal norm SBP operator allows us to manipulate the time derivative into

$$\mathbf{w}^T\mathcal{P}\mathbf{u}_t = \mathbf{1}^T P\mathbf{S}_t \tag{19}$$

where $\mathbf{S}$ is the entropy. We can rewrite the semi-discrete entropy equation as

$$\frac{d}{dt}\mathbf{1}^T\mathcal{P}\mathbf{S}_t = -\mathbf{w}^T\Delta\bar{\mathbf{f}} + \mathbf{w}^T\mathbf{g}^{int} + \mathbf{w}^T\mathbf{g}^{bnd}. \tag{20}$$

This equation provides a sufficient condition for the stability of the inviscid flux, and penalty terms.

The entropy consistent inviscid semi-discretization for generalized SBP is defined to satisfy

$$\mathbf{w}^T\mathcal{P}\mathbf{u}_t + \bar{F}|_1 - \bar{F}|_{-1} = \mathbf{w}^T\mathbf{g}^{int} + \mathbf{w}^T\mathbf{g}^{bnd}, \tag{21}$$

---

[*] The SBP operator used to obtain globally third-order accuracy is a (2-4-2) operator, which uses second order boundary and fourth order interior stencils to obtain that order.

where $\bar{F}|_{-1}$ and $\bar{F}|_{1}$ are the entropy flux of the system interpolated onto the left and right boundary and the telescoping property of the SBP operator Eq. (13) is used to establish the expression. If we substitute the semi-discrete form of the governing equations (17) into above, we establish the relation

$$\mathbf{w}^T \Delta\bar{\mathbf{f}} = \mathbf{1}^T \Delta\bar{\mathbf{F}} = \bar{F}|_1 - \bar{F}|_{-1}. \tag{22}$$

This is the condition that the inviscid flux must satisfy for global entropy consistency in generalized SBP. Note that this recovers the global entropy conservation condition for conventional SBP where the first and last flux points are coincident with the first and last solution points

$$\mathbf{w}^T \Delta\bar{\mathbf{f}} = \mathbf{1}^T \Delta\bar{\mathbf{F}} = \bar{F}(u_N) - \bar{F}(u_1).$$

2. Entropy Conservative Inviscid Flux

The high-order entropy conservative inviscid flux for the generalized SBP finite difference scheme is defined in the following relation

$$\Delta\bar{\mathbf{f}}^S = [2Q \circ \mathcal{F}]\,\mathbf{1}, \tag{23}$$

where Q is described in Eq. (16) and $\mathcal{F}$ is a matrix whose row and column entries consists of the second-order two-point entropy conservative inviscid flux [2] and $\circ$ represents the Hadamard product. Theorems that prove that high-order entropy conservative fluxes can be constructed from linear combinations of two-point-entropy conservative fluxes are available in [2]. The high-order entropy conservative flux is written in closed form as

$$\bar{f}_i^S = \sum_{k=i}^{N}\sum_{l=1}^{i} 2\hat{q}_{(l,k)}\bar{f}(u_l,u_k) + \sum_{k=i+1}^{N}\sum_{l=1}^{N} -b_{-1,k}b_{-1,j}\bar{f}(u_l,u_k) + \sum_{k=1}^{i}\sum_{l=1}^{N} b_{1,k}b_{1,j}\bar{f}(u_l,u_k), \quad 1 \le i \le N-1, \tag{24}$$

where $\hat{q}_{(l,k)}$ are the coefficients of

$$\hat{Q} = Q - \frac{1}{2}\mathcal{B},$$

and $\bar{f}(u_l, u_k)$ is a second-order two-point entropy conservative flux of Ismail and Roe [8].

3. Entropy Stability

An analogous condition to Eq. (21) for entropy stability is

$$\mathbf{w}^T \mathcal{P}\mathbf{u}_t + \mathbf{1}^T \Delta\bar{\mathbf{F}} \le \mathbf{w}^T \mathbf{g}^{int} + \mathbf{w}^T \mathbf{g}^{bnd}. \tag{25}$$

If we substitute the semi-discrete conservation law, Eq. (18), into the entropy stability condition above, we find that entropy stable inviscid fluxes must satisfy

$$\mathbf{w}^T \Delta\bar{\mathbf{f}} \ge \mathbf{1}^T \Delta\bar{\mathbf{F}}^S, \tag{26}$$

where $\bar{\mathbf{F}}^S$ is the entropy consistent entropy flux of the system. With Eq. (22), the entropy stability condition is given as

$$\mathbf{w}^T \Delta\bar{\mathbf{f}} \ge \mathbf{w}^T \Delta\bar{\mathbf{f}}^S. \tag{27}$$

where $\bar{\mathbf{f}}^S$ is a numerical flux that satisfies the entropy consistency condition.

Remark on the Comparison Technique This local comparative entropy stability technique [7] used is proven to be entropy stable in [2] for the conventional SBP high-order finite difference WENO scheme and is used to construct the pointwise entropy stable WENO limiter used in this work. However, one ramification of the generalized SBP is we can no longer prove entropy stability this way due to the non-collocated nature of the boundary solution and flux points. Note that the entropy stability of the generalized SBP is valid in an infinite domain case, *i.e.* periodic domain. We are actively seeking a proof. The comparison approach, without proof, for the generalized SBP operator has been used in this work without stability issues.

D. Entropy Stable WENO Scheme

The entropy stable WENO scheme was introduced for high-order finite difference schemes in [2] for finite domain application. A thorough implementation detail for entropy stable WENO including the formal boundary closure can be found in [9] and for the (2-4-2) WENO operator in [10, 11]. In order to apply WENO as a main dissipative mechanism in high-order finite difference schemes, it is important to cast the scheme in flux form, as shown in Eq. (17). The inviscid fluxes used in the form are called the target fluxes, which have the desired order of accuracy.

$$\bar{f}_i^S = \sum_{l=1}^{n_s} \bar{d}_i^k \bar{f}_i^{S_l}, \quad 0 \leq i \leq N-1, \tag{28}$$

where $n_s = 4$ is the number of candidate stencils, $\bar{f}_i^{S_l}$ are the candidate fluxes, and $\bar{d}^l$ are the target weights.

In WENO, the data across discontinuities are prevented from being used in the flux interpolation [12]. We utilize a nonlinear weight which can place negligible impact when discontinuities are encountered [11], and it is evaluated as follows.

$$\bar{\omega}_i^l = \frac{\bar{\alpha}_i^l}{\sum_j \bar{\alpha}_i^j}, \quad \bar{\alpha}_i^l = \bar{d}_i^l \left(1 + \frac{\bar{\tau}_i^l}{\bar{\beta}_i^l + \bar{\epsilon}_i}\right), \quad l = 1, \ldots, n_s \tag{29}$$

where $\bar{\tau}_i$ is a full stencil smoothness measure, $\bar{\beta}_i^l$ is a candidate stencil smoothness measure, and $\bar{\epsilon}_i$ is a scaling parameter. The full stencil smoothness measure is

$$\bar{\tau}_i = \sum_{l=1}^{n_\tau} \left(\frac{\partial^{2p-1} u(\bar{x}_i)}{\partial x^{2p-1}} (\delta x)^{2p-1}\right)^2, \quad n_\tau = n_s - p. \tag{30}$$

And the candidate stencil smoothness measure is

$$\bar{\beta}_i^l = \sum_{m=1}^{p-1} (\delta x)^{2m} \left(\frac{\partial^m \phi_i^l(\bar{x}_i)}{\partial x^m}\right)^2, \tag{31}$$

where ϕ_i^l is a unique $p-1$ order polynomial fit of the solution over the candidate stencil. Then, the WENO flux is

$$\bar{f}_i^W = \sum_{l=1}^{n_s} \bar{\omega}_i^l \bar{f}_i^{S_l}. \tag{32}$$

The entropy stable WENO method must satisfy the entropy stability condition, Eq. (27)

$$(w_{i+1} - w_i)^T (\bar{f}_i^{SSW} - \bar{f}_i^S) \leq 0, \quad 0 \leq i \leq N-1, \tag{33}$$

where $\bar{f}_i^{SSW}$ is the entropy stable WENO flux and $\bar{f}^S$ is the entropy consistent inviscid flux described in Section III.C.2. The entropy stable limiting procedure that satisfies this condition is

$$\bar{f}_i^{SSW} = \bar{f}_i^W + \delta(\bar{f}_i^S - \bar{f}_i^W), \quad \delta = \frac{\sqrt{b^2 + c^2} - b}{\sqrt{b^2 + c^2}}, \quad b = (w_{i+1} - w_i)^T (\bar{f}_i^S - \bar{f}_i^W), \quad c = 10^{-12} \tag{34}$$

where b is the entropy stability comparison technique and derived from Eq. (27).

IV. Generalized Entropy Stable WENO Finite Differences for Multi-Block Domains

Defining WENO flux across a multi-block interface in the conventional high-order finite difference scheme is difficult due to the collocated flux and solution points on the boundary point. The conventional high-order finite difference scheme satisfying the SBP property defines flux points to be collocated on the domain boundary. While it is possible to extend the entropy stable SAT penalty approach across discontinuous interfaces, the resulting multi-domain coupling becomes weak.

In the generalized SBP, the cell-centered high-order finite difference scheme derived from Sec. III can result in naturally stronger multi-domain coupling. To demonstrate the difference, we illustrate two types of multi-block stencils in Fig. 1. The conventional high-order finite difference stencil is shown in Fig. 1a where the solution points and the flux points of two neighboring blocks coincide at the interface. In the cell-centered high-order finite difference stencil, Fig. 1b, on the other hand, the solution and flux points no longer coincide at the interface leaving a clear choice to define an interface flux.

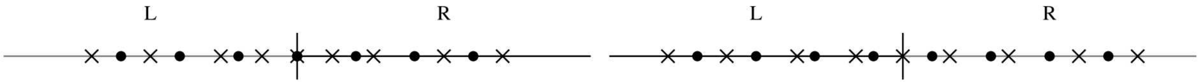

(a) Node-centered **(b) Cell-centered**

Fig. 1 Configurations of the conventional node-centered and cell-centered high-order finite difference stencils at a multi-block interface. The left, L, and the right, R, block are separated by an interface denoted by a vertical line. Solution points and flux points are denoted by ($\bullet$) and ($\times$), respectively. Flux point locations are not to scale.

A. Entropy Stable Multi-Block Interface Penalty

We first describe the global differencing operator for a two-block configuration. The first derivative operators for the left and right block can be formed into the following global operator

$$Q = \begin{bmatrix} Q_L & 0 \\ 0 & Q_R \end{bmatrix}, \tag{35}$$

From this, the multi-block domain telescopic flux form, Eq. (6), is constructed as follows.

$$\begin{bmatrix} \Delta\bar{\mathbf{f}}_L \\ \Delta\bar{\mathbf{f}}_R \end{bmatrix} = Q \begin{bmatrix} \mathbf{f}_L \\ \mathbf{f}_R \end{bmatrix} \tag{36}$$

In this present form, the left and right block solutions are completely independent as no interface coupling has been sought. This global differencing operator can be made nearly skew-symmetric by introducing the interface penalty matrix.

$$\mathcal{G} = \begin{bmatrix} -\frac{1}{2}\mathbf{b}_1^L\mathbf{b}_1^{L^T} & \frac{1}{2}\mathbf{b}_1^L\mathbf{b}_{-1}^{R^T} \\ -\frac{1}{2}\mathbf{b}_{-1}^R\mathbf{b}_1^{L^T} & \frac{1}{2}\mathbf{b}_{-1}^R\mathbf{b}_{-1}^{R^T} \end{bmatrix} \tag{37}$$

where $\mathbf{b}_1^L$ is a boundary interpolation vector that belongs to the left block, and $\mathbf{b}_{-1}^R$ is a vector that belongs to the right block. The global two-block nearly skew-symmetric undivided differencing operator is

$$\Delta\bar{\mathbf{f}} = (Q + \mathcal{G}) \begin{bmatrix} \mathbf{f}_L \\ \mathbf{f}_R \end{bmatrix}. \tag{38}$$

This general form can be used to describe the interface penalty for both conventional and cell-centered high-order finite difference method. In what follows, we describe the entropy stable multi-block interface penalty and the entropy stable WENO method in multi-block domain.

B. Generalized Entropy Stable Multi-Block Interface Penalty

At the multi-block domain interface, the general form of the interface penalty is,

$$\begin{aligned} \mathbf{g}^{int} = & \Big\{\Big(-\mathbf{b}_1^L\mathbf{b}_1^{L^T} \circ \bar{\mathbf{f}}^S(\mathbf{u},\mathbf{u}) + \mathbf{b}_1^L\mathbf{b}_{-1}^{R^T} \circ \bar{\mathbf{f}}^S(\mathbf{u},\mathbf{u})\Big) \\ & \qquad -\frac{1}{2}\mathbf{b}_1^L\mathbf{R}|\Lambda|\mathbf{R}^T\Big(\mathbf{b}_1^{L^T}\mathbf{w} - \mathbf{b}_{-1}^{R^T}\mathbf{w}\Big)\Big\} \\ & - \Big\{\Big(-\mathbf{b}_{-1}^R\mathbf{b}_1^{L^T} \circ \bar{\mathbf{f}}^S(\mathbf{u},\mathbf{u}) + \mathbf{b}_{-1}^R\mathbf{b}_{-1}^{R^T} \circ \bar{\mathbf{f}}^S(\mathbf{u},\mathbf{u})\Big) \\ & \qquad -\frac{1}{2}\mathbf{b}_{-1}^R\mathbf{R}|\Lambda|\mathbf{R}^T\Big(\mathbf{b}_{-1}^{R^T}\mathbf{w} - \mathbf{b}_1^{L^T}\mathbf{w}\Big)\Big\}, \end{aligned} \tag{39}$$

where $\circ$ denotes a Hadamard product of matrices and $\bar{\mathbf{f}}^S$ is an entropy consistent numerical flux, which is non-dissipative. As a result, a Roe-type dissipation term can be added to introduce additional dissipation at the interface. The Roe-type dissipation requires a symmetric decomposition of the flux Jacobian, $\mathbf{A} = \mathbf{R}|\Lambda|\mathbf{R}^T$, which is made possible by utilizing entropy variables, $\mathbf{w}$. Note that this generalized form of entropy stable multi-block interface penalty recovers the interface penalty formulation for the conventional high-order finite difference scheme. This form of the interface penalty is a generalized approach shown in [6].

C. Entropy Stable WENO for Interface

For cell-centered high-order finite differences, the flux and solution points do not coincide at the multi-block interface as demonstrated graphically in Fig. 1b, and we can leverage this property to devise a WENO scheme across an interface. The SBP boundary closure determines the number of unique boundary points. For a third-order high-order finite difference method, four boundary points from both the left and right blocks are required for closure. This suggests that the number of candidate stencils for the interface WENO method is $n_s = 8$, instead of $n_s = 4$ required for a single-block domain. The extension of the formal boundary closure in [9] is made to derive necessary interpolation operator and nonlinear weights for the interface operator.

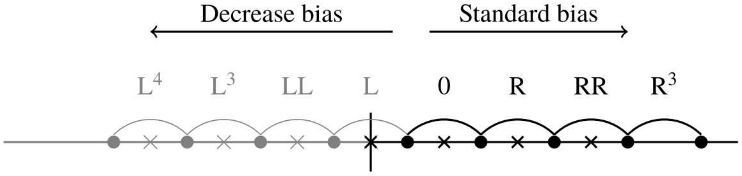

Fig. 2 At the multi-block interface, the WENO flux at 0 flux point is calculated using the stencil biasing mechanic that places larger influence on the candidate stencils that belong in the same block domain as the flux point being considered. Flux points are (×) **and solution points are** (•)**.**

In addition, the stencil biasing introduced in Section III.D must also be altered in order to provide an appropriate upwind biasing. In Eq. (29), the biasing is based on a four candidate stencil configuration. However, in the entropy stable interface WENO, there are eight candidate stencils. One way to introduce upwind biasing is to assign different weights to upwind and downwind stencils. For the right-going wave, as illustrated in Fig. 2, we can modify the weight biasing as

$$\bar{\alpha}_i^l = \begin{cases} \bar{d}_i^l \left(1 + \frac{\bar{\tau}_i^l}{\bar{\beta}_i^l + \bar{\epsilon}_i}\right), & \text{if } l \in [0, R, RR, R^3] \\ \gamma \bar{d}_i^l \left(1 + \frac{\bar{\tau}_i^l}{\bar{\beta}_i^l + \bar{\epsilon}_i}\right), & \text{if } l \in [L, LL, L^3, L^4] \end{cases}, \quad l = 1, \ldots, n_s, \tag{40}$$

where $\gamma \leq 1$ is a scaling factor to reduce the influence of the neighboring block stencils in the biasing process. The left going wave case is similarly treated.

V. Numerical Results

A. Verification

1. Method of Manufactured Solution - Euler Verification

The method of manufactured solution (MMS) is used to verify the inviscid discretization in the Euler equations. The equation we want to solve includes a source term

$$\mathbf{u}_t + \mathbf{f}_x = \mathbf{s}, \tag{41}$$

where the conserved variable vector is $\mathbf{u} = (\rho, \rho u, \rho E)^T$, the conserved flux vector is $\mathbf{f} = (\rho u, \rho u^2 + p, \rho u H)^T$, and the source term is $\mathbf{s}$. For the initial condition

$$(\rho, u, T) = (2 + \cos(\pi x), 2 + \cos(\pi x), 2 + \cos(\pi x)), \tag{42}$$

the source term is

$$\mathbf{s} = -\begin{pmatrix} 2\pi \sin(\pi x)(\cos(\pi x) + 2) \\ \pi \sin(\pi x)(\cos(\pi x) + 2)(2R + 3\cos(\pi x) + 6) \\ \pi \sin(\pi x)((\cos(\pi x) + 2)^2(3c_p + 2\cos(\pi x) + 4), \end{pmatrix}, \tag{43}$$

where R is the gas constant and c_p is the specific heat constant. The computational domain is defined $-1 \leq x \leq 1$ and the simulation is ran to $t = 0.1$. We ran the Euler code in both a single and a two-block configuration to verify the accuracy of entropy stable WENO scheme.

Table 1 Entropy stable cell-centered high-order finite difference WENO scheme error convergence in a single block, Euler MMS

N	h	$\epsilon_2(\rho)$	Rate	$\epsilon_2(u)$	Rate	$\epsilon_2(T)$	Rate
32	6.06E-02	1.02E-03		5.96E-03		5.28E-01	
64	3.08E-02	5.67E-05	4.27	1.07E-03	2.53	5.66E-02	3.30
128	1.55E-02	4.09E-06	3.84	8.77E-05	3.66	4.29E-03	3.76
256	7.78E-03	2.80E-07	3.89	5.91E-06	3.91	2.87E-04	3.92
512	3.90E-03	1.81E-08	3.96	3.80E-07	3.97	1.83E-05	3.98

Table 2 Entropy stable cell-centered high-order finite difference WENO scheme error convergence in a two-block domain, Euler MMS

2N	h	$\epsilon_2(\rho)$	Rate	$\epsilon_2(u)$	Rate	$\epsilon_2(T)$	Rate
32	5.88E-02	9.03E-03		3.92E-02		3.51E+00	
64	3.03E-02	3.57E-04	4.87	1.22E-03	5.23	3.63E-01	3.42
128	1.54E-02	3.04E-05	3.64	9.73E-05	3.73	2.92E-02	3.72
256	7.75E-03	2.10E-06	3.90	6.89E-06	3.86	1.97E-03	3.93
512	3.89E-03	1.35E-07	3.98	4.36E-07	4.01	1.27E-04	3.98

2. Viscous Shock - Navier Stokes Verification

A viscous shock problem [13] is used to verify the accuracy of the Navier-Stokes discretization, inviscid and viscous discretizations. The governing equations now must include the viscous flux vector

$$\mathbf{f}_k^{(v)} = (0, \tau_{1k}, \tau_{2k}, \tau_{3k}, \tau_{ik} v_i - q_k)^T, \tag{44}$$

where the heat flux is $q_k = -\kappa T_{x_k}$ and the shear stress tensor is

$$\tau_{ij} = \mu \left((v_i)_{x_j} + (v_j)_{x_i} - \delta_{ij} \frac{2}{3} (v_l)_{x_l} \right), \tag{45}$$

and μ is the fluid viscosity. This form of governing equation is used again for the multi-dimensional Taylor Green vortex problem later on. Details regarding the discretization and stability of the viscous terms are detailed in [13].

A convecting viscous shock with a constant width initially positioned at $x_0 = 0.5$ in a one-dimensional domain $0 < x < 2$ and is simulated until $t = 0.1$ at which point an exact solution can be evaluated, see [13] for the derivation of this verification problem. The viscosity value of $\mu = 5$ was used for a freestream Mach number flow $Ma = 2.23$. We show the L_2 norm error of primitive variables for a single and a multi-block domain configuration. In the multi-block case, the domain was divided into two with the multi-block interface located at $x = 1$. We observe the expected third-order convergence rate in both cases.

Table 3 Entropy stable cell-centered high-order finite difference WENO scheme error convergence in a single block, viscous shock

N	h	$\epsilon_2(\rho)$	Rate	$\epsilon_2(u)$	Rate	$\epsilon_2(T)$	Rate
64	3.08E-02	9.35E-02		3.76E+02		7.92E+05	
128	1.55E-02	4.79E-02	0.977	1.93E+02	0.971	4.08E+05	0.969
256	7.78E-03	1.17E-02	2.04	4.73E+01	2.04	1.00E+05	2.04
512	3.90E-03	1.45E-03	3.03	5.91E+00	3.01	1.27E+04	2.99

Table 4 Entropy stable cell-centered high-order finite difference WENO scheme error convergence in a two-block domain, viscous shock

2N	h	$\epsilon_2(\rho)$	Rate	$\epsilon_2(u)$	Rate	$\epsilon_2(T)$	Rate
64	3.03E-02	1.19E-01		4.77E+02		1.00E+06	
128	1.54E-02	6.89E-02	0.803	2.79E+02	0.792	5.89E+05	0.784
256	7.75E-03	1.71E-02	2.03	6.91E+01	2.03	1.46E+05	2.03
512	3.89E-03	2.09E-03	3.05	8.52E+00	3.04	1.82E+04	3.02

B. One-Dimensional Test

1. Shock tube

The Sod shock tube problem [14] is considered here to demonstrate the shock capturing capability of different schemes. The initial condition is

$$(\rho, u, p) = \begin{cases} (1, 0, 1), & \text{if } x < 0.5 \\ (0.125, 0, 0.1), & \text{if } x \geq 0.5, \end{cases} \tag{46}$$

and the computational domain is $0 < x < 1$. For this problem, we compare the conventional entropy stable node-centered and the cell-centered high-order finite difference WENO schemes in a multi-block configuration. The entropy stable penalty used in the node-centered high-order finite difference WENO is discussed in [2]. In cell-centered high-order finite difference WENO, the entropy stable WENO method described in Section IV.C is used to across two different domains.

The density solution profile is shown in Fig. 3. The computational domain is divided into three sub-domains with interfaces indicated by vertical dashed lines. Comparing with the reference solution, both WENO schemes resolve the contact discontinuity and the shock well. Across the multi-block interface near the contact discontinuity, the conventional node-centered high-order finite difference WENO scheme suffers from a slight oscillation as shown in Fig. 3b.

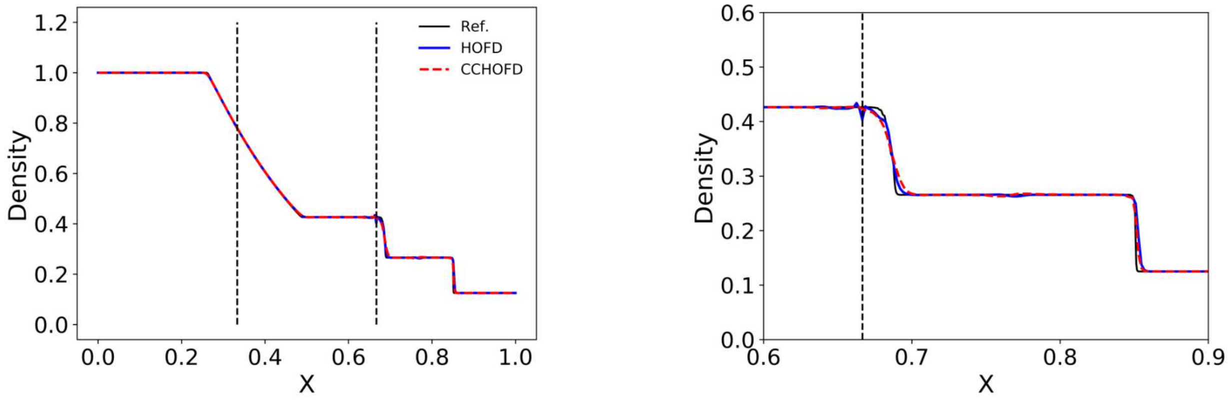

(a) Density **(b) Density close up near the contact discontinuity**

Fig. 3 Sod shock tube density profile of the conventional high-order finite difference (HOFD) and cell-centered high-order finite difference (CCHOFD), $N = 512$**,** $t_f = 0.25$**. The computational domain is divided into three sub-domains with interfaces indicated by vertical dashed lines.**

2. Shu Osher Problem

The Shu Osher problem [15] is an interaction of a strong normal shock front moving into a standing entropy wave fluctuation. It is used to assess the numerical scheme's ability to resolve turbulence-like features in a one-dimensional flow. The initial condition is

$$(\rho, u, p) = \begin{cases} (3.857143, 2.629369, 10.3333), & \text{if } x < -4.0 \\ (1 + 0.2\sin(5x), 0, 1), & \text{if } x \geq -4.0. \end{cases} \tag{47}$$

In Fig. 4, the overall solution and the solution near the shock interaction region for the Shu Osher problem are shown for a two-block configuration. The block interface is located at $x = 0$. Both schemes resolve the smooth portions of the solution well. However, the difference between the conventional and cell-centered high-order finite differences becomes clear in the shock interaction region. Neither scheme resolves the oscillatory portion of the solution well. We notice that the cell-centered high-order finite difference WENO reproduces the reference solution marginally better than the conventional high-order WENO scheme near the shock front, Fig. 4b. Both schemes show some numerical artifact produced as a result of the multi-block interface.

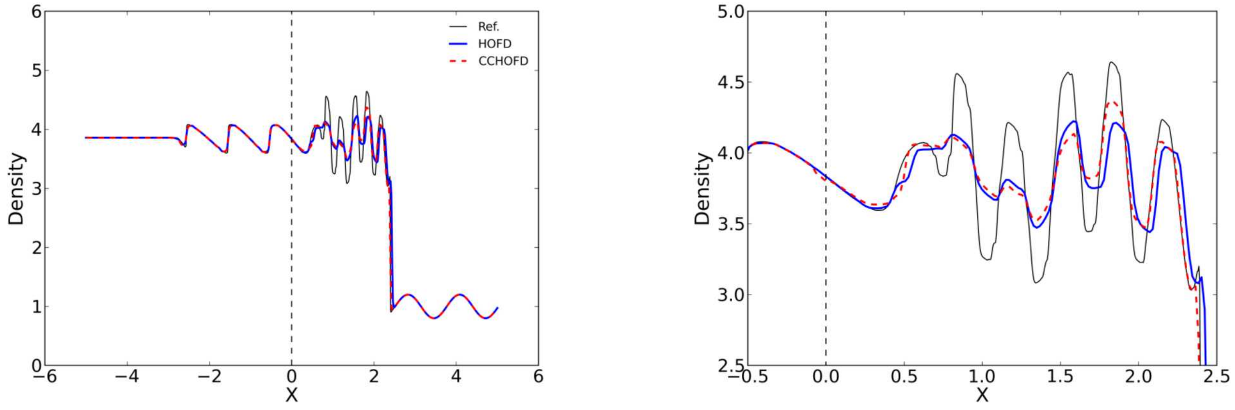

(a) Density **(b) Density close up**

Fig. 4 Shu Osher solution of the conventional high-order finite difference (HOFD) and cell-centered high-order finite difference (CCHOFD) $N = 512$**,** $t_f = 1.8$**. The computational domain is divided at** $x = 0$**, and the interface is denoted by a black dashed line. The reference solution uses** $N = 2000$ **cells.**

C. Woodward Colella

The Woodward Colella problem [16] is a problem containing the interaction of two strong shocks. Two strong shock waves formed at two fluid interfaces collide, then form a strong right-going shock wave. The right-going shock wave reflect off an inviscid wall. The boundary condition on both boundaries is set to a slip wall condition [4]. This problem tests not only the shock capturing capability of a numerical scheme but also the stability of a numerical wall boundary condition. The initial condition is

$$(\rho, u, p) = \begin{cases} (1, 0, 1000), & \text{if } x < 0.1 \\ (1, 0, 100), & \text{if } 0.1 \leq x < 0.9 \\ (1, 0, 0.01), & \text{if } x \geq 0.9. \end{cases} \tag{48}$$

For the multi-block problem shown in Fig. 5, the interface is located in the middle of the computational domain. This test problem is more revealing than the previous two because the solution interacts in two different ways; (i) with the multi-block interface and (i) the slip wall. The results are shown at $t = 0.04$ after the initial disturbance reflects off the wall and interact with each other.

As shown in Figs. 5 and 6, the conventional high-order finite difference WENO scheme suffers significantly and deviates from the expected reference solution. Both schemes suffer from numerical noise due to the strong shock interaction in Fig. 6. However, the cell-centered high-order finite difference scheme demonstrates superior shock capturing behavior.

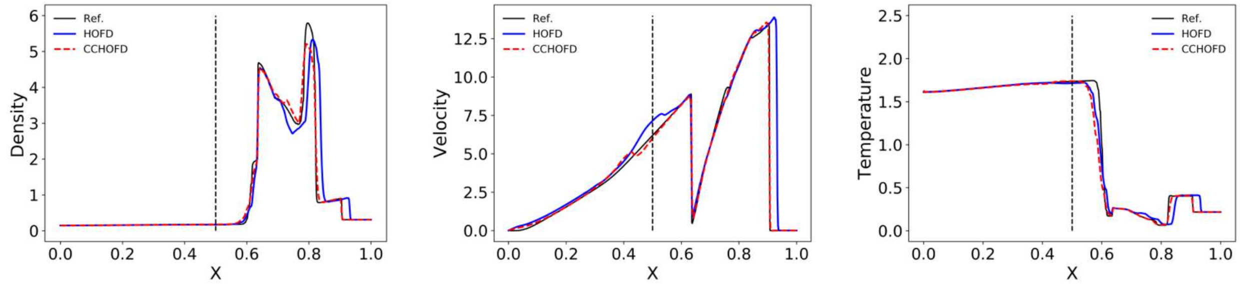

(a) Density **(b) Velocity** **(c) Temperature**

Fig. 5 Woodward Colella solution of the conventional high-order finite difference (HOFD) and cell-centered high-order finite difference (CCHOFD), $N = 512$, $t_f = 0.04$. The multi-block interface is located at $x = 0.5$. The reference solution is computed with $N = 2048$ cells.

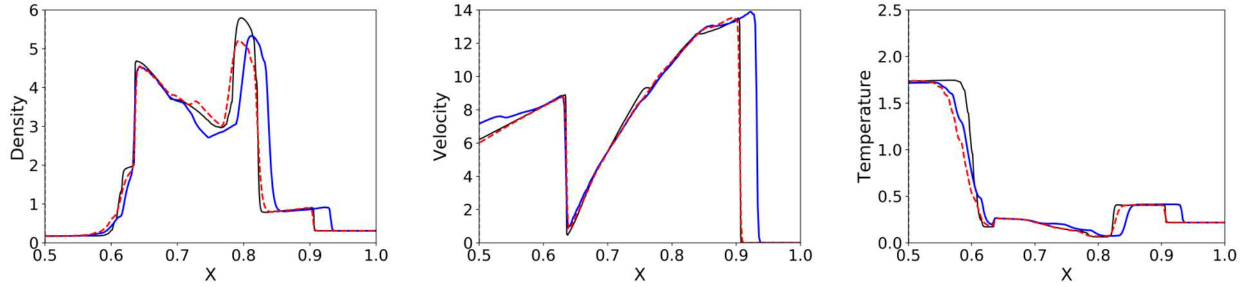

(a) Density **(b) Velocity** **(c) Temperature**

Fig. 6 Close up of the Woodward Colella solution $N = 512$, $t_f = 0.04$. The multi-block interface is located at $x = 0.5$. The reference solution is computed with $N = 2048$ cells.

D. Multi-Dimensional Test

In the following section, we demonstrate stability and accuracy of the cell-centered high-order entropy stable WENO scheme in multi-dimensional problems.

1. Two-Dimensional Sod Shock tube

The two-dimensional Riemann problem is described by,

$$(\rho, u, v, p) = \begin{cases} (1, 0, 0, 1), & \text{if } r \leq 0.4 \\ (0.125, 0, 0, 0.1), & \text{if } r > 0.4, \end{cases} \tag{49}$$

where the radius is defined as $r = \sqrt{x^2 + y^2}$ and the computational domain is $[-1 < (x, y) < 1]$. This is a two-dimensional analogue of the Sod shock tube problem considered in one dimension. This test demonstrates the shock capturing capability in a multi-block domain in multi-dimensions.

A Cartesian grid with regularly spaced 80^2 cells is used to simulate the problem with the cell-centered high-order finite difference WENO scheme for a single-block and multi-block configurations. In Fig. 7, density radial solutions at $t = 0.25$ are shown for the single and multi-block configuration. For the multi-block configuration, the single block mesh was sub-divided into 16 equally sized blocks. For the shown resolution, 80^2 mesh, each sub-block contains 20^2 cells. Both results predict all relevant flow features shown in the reference solution.

In addition to demonstrating the robust shock capturing ability on a multi-block mesh, the result also illustrates the scheme's ability to preserve the solution radial isotropy. Simulating a radially symmetric problem on a cartesian grid will result in some grid induced error/anisotropy. As shown, the multi-block entropy stable WENO result shows a wider density radial profile while the single block result does not exhibit as severe solution anisotropy. Along with the fact there are multi-block interfaces, reduced dissipation across interface may have introduced grid induced anisotropy.

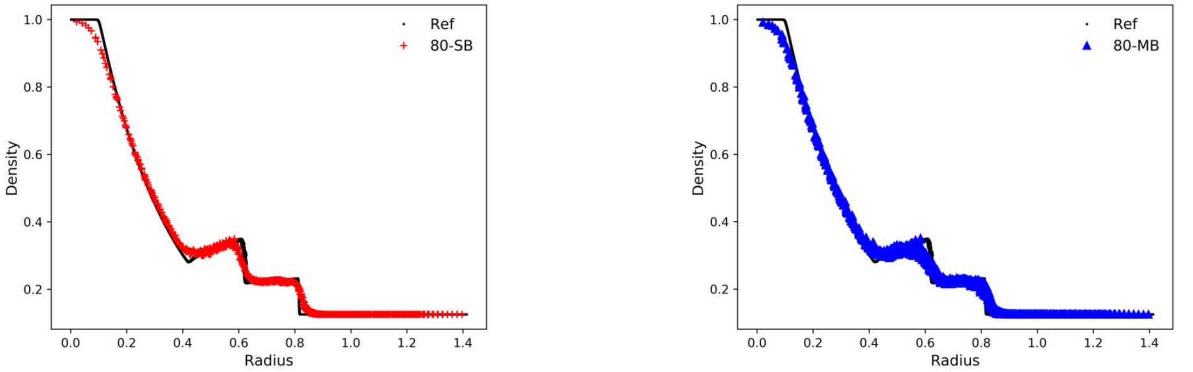

(a) 80^2 **mesh, a single block**

(b) 80^2 **mesh equally divided into 16 sub-blocks**

Fig. 7 Radial density plot, $t = 0.25$**. Reference solution evaluated on a** 1280^2 **mesh.**

2. Taylor Green Vortex

The Taylor Green Vortex problem is a three-dimensional problem which contains cascading vortices that monotonically decrease in scale with time. It is used to compare the accuracy and robustness of a scheme. We use this problem to assess the stable property across multi-block interfaces in three dimensions. The problem is solved on a periodic domain $[-\pi L \leq (x, y, z) \leq \pi L]$ and the initial condition is given by the following analytical expressions,

$$\rho(x, y, z, 0) = 1.0 \tag{50}$$

$$u(x, y, z, 0) = V_0 \sin\left(\frac{x}{L}\right) \cos\left(\frac{y}{L}\right) \cos\left(\frac{z}{L}\right) \tag{51}$$

$$v(x, y, z, 0) = -V_0 \cos\left(\frac{x}{L}\right) \sin\left(\frac{y}{L}\right) \cos\left(\frac{z}{L}\right) \tag{52}$$

$$w(x, y, z, 0) = 0 \tag{53}$$

$$p(x, y, z, 0) = 1.0 + \frac{\gamma M_0^2}{16} \left(\cos\left(\frac{2x}{L}\right) + \cos\left(\frac{2y}{L}\right)\right) \left(\cos\left(\frac{2z}{L} + 2\right)\right), \tag{54}$$

where the Mach number, $M_0 = 0.1$ and the Reynolds number is set to 1600.

The direct numerical simulation result was obtained from a spectral method on a 512^3 mesh, which was provided as part of the third international workshop on high-order CFD methods [17]. The single block mesh consists of 64^3 cells. For this comparison, we divide the single block mesh into equally sized 8 sub-blocks, thus each block contains 32^3 cells, to compare the single and multi-block entropy conservative high-order finite differences. We compare several schemes, namely, entropy conserving high-order finite differences in single and multi-blocks, entropy stable hybrid WENO high-order finite differences in single and multi-blocks, and a low-dissipative fourth-order finite volume using the Subbareddy and Candler flux [18] with a Mach number-based shock switch also included for reference.

In order to assess the accuracy of schemes, we calculate several quantities to compare: the total integrated kinetic energy, its dissipation rate, and enstrophy. The total kinetic energy is

$$E_k = \frac{1}{\rho\Omega}\int_\Omega \rho\frac{v_i v_i}{2}d\Omega, \tag{55}$$

where v_i is the velocity vector. And the total enstrophy is

$$\zeta = \frac{1}{\rho\Omega}\int_\Omega \rho\frac{\omega_i \omega_i}{2}d\Omega, \tag{56}$$

where ω_i is the vorticity. This measure can be used as a theoretical kinetic energy dissipation rate, in addition to the discrete kinetic energy dissipation rate evaluated from the kinetic energy [19].

The shock capturing capability of a scheme often comes at the cost of degraded turbulence resolving capability. This is because shocks and other strong nonlinear features require numerical dissipation for stability, which has a natural tendency to smear out structures in high-fidelity flow simulations. In Fig. 8, we show the kinetic energy of entropy stable high-order finite difference WENO. In this case, WENO is applied everywhere in the flow and consequently is manifested into lower kinetic energy values. For this reason, we have developed a hybrid WENO scheme that addresses the issue of increased numerical dissipation by turning the dissipation mechanism on only when needed. This is achieved by a shock sensor based on the dilation of the flow [13, 20]. Our nonlinear stabilization method only activates when the negative rate of dilation is observed.

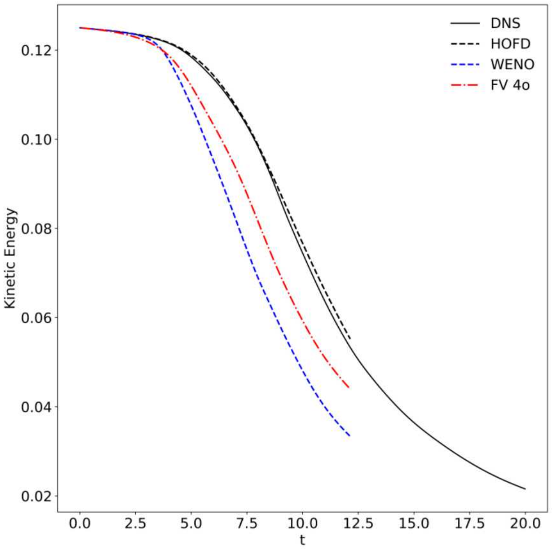

Fig. 8 Total integrated kinetic energy comparison between entropy stable high-order finite difference (HOFD), WENO (WENO), and a fourth-order finite volume (FV 4o)

Total integrated kinetic energies for various schemes are presented in Fig. 9. Total kinetic energy results for entropy conserving high-order finite difference schemes show good agreement with the direct numerical simulation result. There is a small variation between entropy conserving high-order finite difference and the hybrid WENO scheme for both single and multi-block configurations. The finite volume simulation, which is a kinetic energy preserving scheme, however, cannot accurately simulate the kinetic energy dissipation rate compared to the entropy conserving or stable schemes.

Dissipation rates are presented in Fig. 10. The kinetic energy dissipation rate is simply evaluated by taking a central difference of the total integrated kinetic energy of each scheme. The total enstrophy is calculated according to the formula. We notice that all finite difference results replicate the DNS result well whereas there is some discrepancy in the finite volume result. In all mentioned results, there is little to no difference between the single and multi-block simulations.

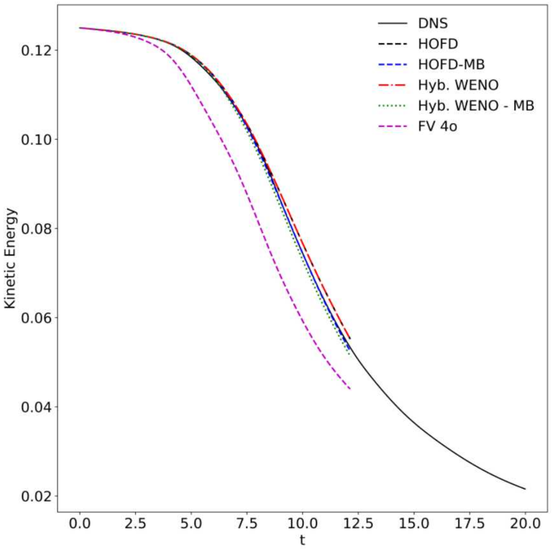

Fig. 9 Total integrated kinetic energy comparison between entropy stable high-order finite difference (HOFD), and multi-block (HOFD-MB), hybrid WENO (Hyb. WENO), and multi-block (Hyb. WENO-MB), and a fourth-order finite volume (FV 4o)

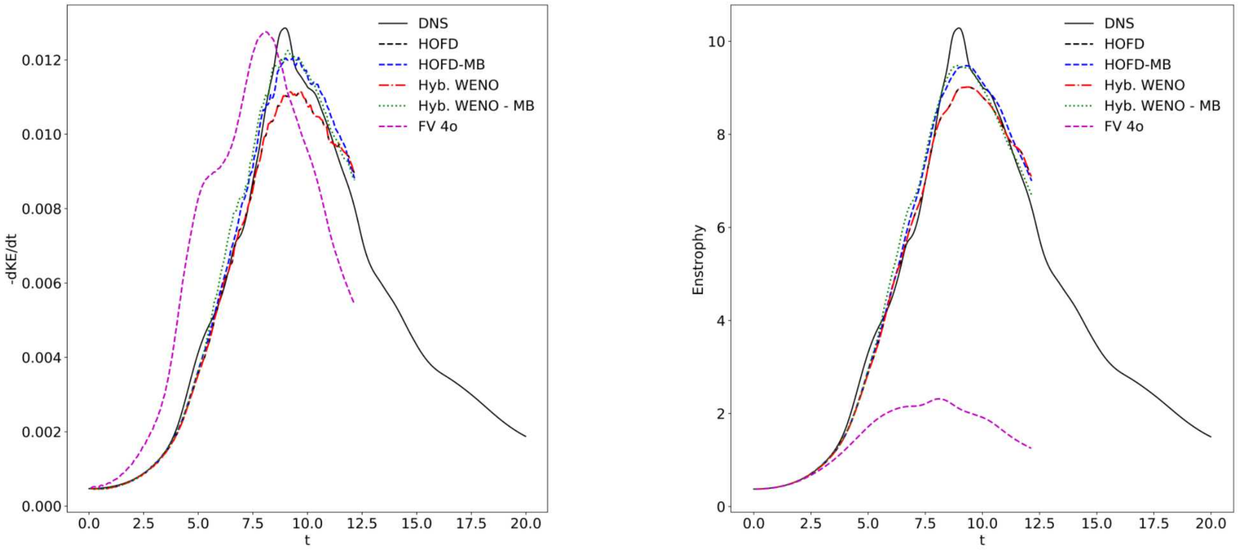

(a) Kinetic energy dissipation rate

(b) Total integrated enstrophy

Fig. 10 Dissipation rate comparison between entropy stable high-order finite difference (HOFD), and multi-block (HOFD-MB), hybrid WENO (Hyb. WENO), and multi-block (Hyb. WENO-MB), and a fourth-order finite volume (FV 4o)

VI. Conclusion and Future Directions

In this paper, we have presented the generalized framework for entropy conservative finite differences and entropy stable WENO scheme in multi-block domains. We first defined a generalized SBP-SAT framework which allows us to construct a cell-centered high-order finite difference scheme. The newly developed cell-centered formulation not only is conservative, consistent and can be proven entropy conservative. Additionally, the generalized SBP-SAT framework can provide a stronger coupling at multi-block interfaces by introducing a skew-symmetric interface penalty operator. From this, both a generalized entropy stable multi-block interface penalty and an entropy stable WENO can be designed. The proclaimed benefit of generalized entropy stable WENO across multi-block interfaces is that the operator is no longer weakly coupled due to uniquely defined cell-centered solution points at the domain boundary.

We have demonstrated the robustness and accuracy of the new cell-centered high-order finite difference and entropy stable WENO scheme with one-dimensional problems. On the Sod shock tube and the Shu Osher problem, both the conventional and the cell-centered high-order finite difference schemes exhibited similar results. On the Woodward Colella problem, however, we observed that the conventional entropy stable high-order finite difference WENO scheme exhibited a wrong shock speed after passing through the multi-block interface. The Woodward Colella problem is a difficult problem, and consequently, the cell-centered entropy stable high-order finite difference WENO scheme also suffered from numerical oscillation on and near the block interface. Overall, we have shown a favorable stability and shock capturing property of the new cell-centered high-order finite difference WENO scheme.

In multiple dimensions, we have considered a two-dimensional analogue of the Sod shock tube problem. This problem showed that the entropy stable cell-centered high-order finite difference WENO is stable for multiple blocks. However, it exhibited a well-known grid imprinting issue. While it is an issue, we believe that the benefits of having a robust multi-domain treatment would outweigh the slight numerical artifact from interfaces. In the Taylor Green vortex problem, we observed that the entropy stable cell-centered high-order finite difference WENO is both stable and accurate for a three-dimensional turbulent vortex cascade problem in a single and multi-block configuration. But it was too dissipative to resolve fine turbulent structures. We have introduced a hybrid WENO scheme and demonstrated improved turbulent scale resolving capability along with stability. The entropy stable schemes performed and compared well against a well-established kinetic energy preserving finite volume scheme.

There are some points to address going forward. The entropy stable WENO stencil biasing can be studied in depth. As mentioned, the candidate stencil width for the WENO scheme across multi-block interface is 8 due to the boundary closure condition. For a third-order scheme, this number is excessive, and the stencil biasing mechanics becomes a bit ambiguous and heuristic in nature. A more robust stencil biasing mechanic needs to be developed. We have seen in two-dimensional Sod shock tube that multi-block scheme induces grid related anisotropy. This may be due to the non-dissipative interface penalty. Even with some of these points to address, the extension to curvilinear multi-block domains is straight-forward. In subsequent works, we plan to extend the current methodology to multi-dimensional curvilinear multi-block domains with aforementioned improvements for high-speed compressible flow applications.

VII. Acknowledgments

Sandia National Laboratories is a multimission laboratory managed and operated by National Technology and Engineering Solution of Sandia LLC, a wholly owned subsidiary of Honeywell International Inc. for the U.S. Department of Energy's National Nuclear Security Administration under contract DE-NA0003525.

This paper describes objective technical results and analysis. Any subjective views or opinions that might be expressed in the paper do not necessarily represent the views of the U.S. Department of Energy or the United States Government.

References

[1] Fernández, D. C. D. R., Boom, P. D., and Zingg, D. W., "A generalized framework for nodal first derivative summation-by-parts operators," *Journal of Computational Physics*, Vol. 266, 2014, pp. 214–239.

[2] Fisher, T. C., and Carpenter, M. H., "High-order entropy stable finite difference schemes for nonlinear conservation laws: Finite domains," *Journal of Computational Physics*, Vol. 252, 2013, pp. 518–557.

[3] Yamaleev, N. K., and Carpenter, M. H., "A family of fourth-order entropy stable nonoscillatory spectral collocation schemes for the 1-D Navier-Stokes equations," *Journal of Computational Physics*, Vol. 331, 2017, pp. 90 – 107. doi:https://doi.org/10.1016/j.jcp.2016.11.039, URL `http://www.sciencedirect.com/science/article/pii/S0021999116306313`.

[4] Svärd, M., and Özcan, H., "Entropy-stable schemes for the Euler equations with far-field and wall boundary conditions," *Journal of Scientific Computing*, Vol. 58, No. 1, 2014, pp. 61–89.

[5] Parsani, M., Carpenter, M. H., and Nielsen, E. J., "Entropy stable wall boundary conditions for the three-dimensional compressible Navier–Stokes equations," *Journal of Computational Physics*, Vol. 292, 2015, pp. 88–113.

[6] Carpenter, M. H., Fisher, T. C., Nielsen, E. J., and Frankel, S. H., "Entropy Stable Spectral Collocation Schemes for the Navier–Stokes Equations: Discontinuous Interfaces," *SIAM Journal on Scientific Computing*, Vol. 36, No. 5, 2014, pp. B835–B867.

[7] Tadmor, E., "Entropy stability theory for difference approximations of nonlinear conservation laws and related time-dependent problems," *Acta Numerica*, Vol. 12, 2003, pp. 451–512.

[8] Ismail, F., and Roe, P. L., "Affordable, entropy-consistent Euler flux functions II: Entropy production at shocks," *Journal of Computational Physics*, Vol. 228, No. 15, 2009, pp. 5410–5436.

[9] Fisher, T. C., Carpenter, M. H., Yamaleev, N. K., and Frankel, S. H., "Boundary closures for fourth-order energy stable weighted essentially non-oscillatory finite-difference schemes," *Journal of Computational Physics*, Vol. 230, No. 10, 2011, pp. 3727–3752.

[10] Carpenter, M. H., Fisher, T. C., and Yamaleev, N. K., "Boundary closures for sixth-order energy-stable weighted essentially non-oscillatory finite-difference schemes," *Advances in Applied Mathematics, Modeling, and Computational Science*, Springer, 2013, pp. 117–160.

[11] Yamaleev, N. K., and Carpenter, M. H., "Third-order energy stable WENO scheme," *Journal of Computational Physics*, Vol. 228, No. 8, 2009, pp. 3025–3047.

[12] Jiang, G.-S., and Shu, C.-W., "Efficient implementation of weighted ENO schemes," *Journal of computational physics*, Vol. 126, No. 1, 1996, pp. 202–228.

[13] Fisher, T. C., "High-order L2 stable multi-domain finite difference method for compressible flows," Ph.D. thesis, Purdue University, 2012.

[14] Sod, G. A., "A survey of several finite difference methods for systems of nonlinear hyperbolic conservation laws," *Journal of computational physics*, Vol. 27, No. 1, 1978, pp. 1–31.

[15] Shu, C.-W., and Osher, S., "Efficient implementation of essentially non-oscillatory shock-capturing schemes," *Journal of computational physics*, Vol. 77, No. 2, 1988, pp. 439–471.

[16] Woodward, P., and Colella, P., "The numerical simulation of two-dimensional fluid flow with strong shocks," *Journal of computational physics*, Vol. 54, No. 1, 1984, pp. 115–173.

[17] "Third international workshop on high-order CFD methods," `https://www.grc.nasa.gov/hiocfd/`, 2015. [Online;].

[18] Subbareddy, P. K., and Candler, G. V., "A fully discrete, kinetic energy consistent finite-volume scheme for compressible flows," *Journal of Computational Physics*, Vol. 228, No. 5, 2009, pp. 1347–1364.

[19] DeBonis, J., "Solutions of the Taylor-Green vortex problem using high-resolution explicit finite difference methods," *51st AIAA Aerospace Sciences Meeting including the New Horizons Forum and Aerospace Exposition*, 2013, p. 382.

[20] Larsson, J., Vicquelin, R., and Bermejo-Moreno, I., "Large eddy simulations of the HyShot II scramjet," *Center for Turbulence Research Annual Research Briefs*, Vol. 2011, 2011.